Marine Structures 81 (2022) 103119

Contents lists available at ScienceDirect

Marine Structures

journal homepage: www.elsevier.com/locate/marstruc

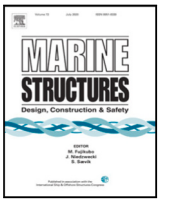

Analysis of fatigue test data of retrieved mooring chain links subject to pitting corrosion

Jorge Mendoza *, Per J. Haagensen, Jochen Köhler

Norwegian University of Science and Technology, Department of Structural Engineering, 7491 Trondheim, Norway

ARTICLE INFO

Keywords:
Fatigue test
Mooring lines
Pitting corrosion
Hierarchical models

ABSTRACT

Fatigue is one of the main failure mechanisms of catenary type mooring lines. Fatigue resistance is affected by a large number of factors. In this paper, the effect of pitting corrosion on the fatigue resistance of mooring lines is empirically estimated. Data from fatigue testing of both new and used chain links are considered. The used chain link samples were retrieved from several offshore floating units. A hierarchical statistical analysis is proposed to effectively use the available information. Mean stress effect is taken into account in the analysis of the data. Results show that the effect of pitting corrosion on the structural reliability of mooring lines is significant.

1. Introduction

Position keeping of offshore oil and gas floating facilities is secured by mooring systems. A mooring system is composed of several lines. Mooring lines typically include mooring chains, often in combination with polyester or wire ropes. An example of a common mooring line configuration with mooring chain and wire rope is shown in Fig. 1. Mooring chains are non-redundant structures, meaning that failure of a link leads to failure of the mooring line. Subsequently, failure of a mooring line results in large replacement costs and, until detected, in an increased risk of failure of the mooring system due to progressive failure.

Fatigue and corrosion deterioration processes are among the most common causes of failure of chain links during operation [1,2]. These two failure mechanisms are treated as weakly coupled phenomena in design standards, such as ISO 19901-7:2013 [3], API RP 2SK [4] and DNVGL-OS-E301 [5]. In these standards, the interaction between corrosion and fatigue is accounted for by considering a corrosion allowance in the fatigue limit state. This is considered to be a major simplification because the interaction between corrosion and fatigue is more complex in nature when pitting corrosion is present [6]. The fatigue-corrosion interaction has been observed to result in significantly lower fatigue lives than what is prescribed in design standards [7–9].

Mild and low-alloy steel components immersed in seawater tend to develop a type of local corrosion known as pitting corrosion. According to Melchers [10], pit growth fundamentally consists of an initial and relatively mild aerobic phase, and an aggressive anaerobic phase. The anaerobic phase is mainly caused by microbial agents such as sulphate-reducing bacteria (SRB), whose growth and activity are highly influenced by the water temperature. This type of surface degradation is particularly present in two sections of the mooring line: (a) in the bottom part where the chain is buried under the sea bed; and (b) in the turret section in which conditions are favourable for marine growth and the subsequent microbial corrosion caused by SRB [7,11]. Gabrielsen et al. [11,12] report observations of mooring chain specimens suffering from significant pitting corrosion after 5 to 20 years in service. They identify the local geometry and the depth of the pits as important factors for fatigue resistance reduction. Furthermore, Kondo [13] shows

* Corresponding author.
E-mail addresses: jorge.m.espinosa@ntnu.no (J. Mendoza), per.haagensen@ntnu.no (P.J. Haagensen), jochen.kohler@ntnu.no (J. Köhler).

https://doi.org/10.1016/j.marstruc.2021.103119
Received 17 March 2021; Received in revised form 13 August 2021; Accepted 1 November 2021
Available online 17 November 2021

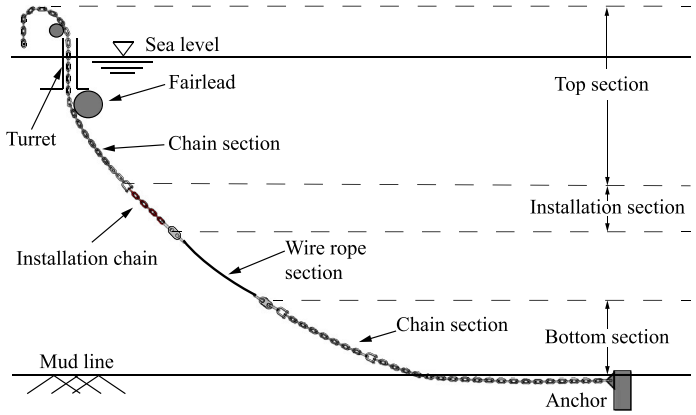

Fig. 1. Example of a typical mooring line of oil and gas platforms in the North Sea and Norwegian Sea.

that local stress concentrations at pits may lead to the development of fatigue cracks and the subsequent crack propagation under cyclic stresses.

In addition to the corrosion condition, recent studies have shown that the nominal mean stress that the mooring chains are subject to may have significant consequences on fatigue resistance [12,14]. This effect is typically unaccounted for in design standards for mooring lines. It should nonetheless be noticed that the fatigue tests used to develop fatigue resistance models in API RP 2SK [4] and DNVGL-OS-E301 [5] were based on a constant high mean stress, which results in conservative practice. The mean stress effect should however be regarded for producing more accurate fatigue resistance models or when a variety of mean stresses are employed for fatigue testing.

Understanding and quantifying the effect of the corrosion condition on fatigue life reduction are relevant for the design and the reassessment of mooring systems, particularly, to inform integrity management decisions, such as inspection planning, repair, and replacement decisions. In the present article, we propose an engineering model to assess the fatigue resistance of mooring lines as a function of their corrosion condition. The proposed model builds on the current common practice, which is briefly outlined hereafter.

Typically, design standards prescribe the use of semiempirical S–N curves to assess the fatigue resistance of steel components, including mooring chains [4,5,15–17]. An S–N curve is a power law that represents the number of fatigue cycles N that a structural component with certain characteristics can survive as a function of the nominal stress range ΔS:

$$N = k \cdot \Delta S^{-m}, \tag{1}$$

where k and m are the model parameters.

Commonly, design standards specify the model parameters of the so-called design curves. The design curve is typically defined as the S–N curve associated with a non-exceedance probability of N given ΔS of 2.28% [18]. S–N models are fitted based on representative experimental data. Because fatigue life is affected by many variables that are not explicitly included in the S–N model, the validity of using a certain design curve in a given design scenario depends on the representativeness of the data employed to develop the curve. This limitation is partially addressed in design standards by providing several S–N curves that aim to cover most practical applications. For example, different design curves are found to be representative for different structural connections and types of welding. Consequently, the S–N model that is developed in the present study is valid for cases for which the analysed data is considered representative.

The proposed S–N curve is developed from the analysis of tension–tension fatigue test data of both new and retrieved full-scale chain segments. We refer to this S–N model as an extended S–N model because, in addition to the stress range, it includes a corrosion indicator as input variable. The obtained fatigue resistance model is used to estimate the effect of pitting corrosion on fatigue resistance. The characterisation of the retrieved specimens and the experimental methods used for fatigue testing are presented in Section 2. The fatigue data is presented in Section 3. The considered specimens are heterogeneous, meaning that they were retrieved from different platforms located in the North Sea and the Norwegian Sea and differ among each other according to several relevant features. In Section 4, we propose the use of a hierarchical method to abstract the causal effect of the corrosion condition on fatigue resistance from the data. The obtained extended S–N model is presented in Section 5. Furthermore, the sensitivity of the inferred model regarding the mean stress effect is studied in that section. The inferred fatigue resistance model is used in a case study in Section 6 to estimate the impact of the corrosion condition on the structural reliability of a mooring chain. The paper concludes with some general remarks and outlook for future research challenges.

2. Materials and experimental methods

Tension–tension fatigue tests of full-scale, studless chain links were conducted to produce the fatigue data. In total, the considered data set consists of 150 data points, see Table 1. The fatigue tests were part of three different test campaigns. Two of them dealt

Table 1
Considered data set, including the platform from where specimens where retrieved. Values in square brackets correspond to [min, max] of the property.

Subset	Platform	Type	Location	Service years	C	# tests
S1	P1	FPSO	bot./instal./top	[12, 20]	[4, 7]	15
	P2	FPSO	top	5	[1, 4]	4
S2	P1	FPSO	top	[10, 12]	[2,6]	7
	P2	FPSO	bot.	18	[4, 7]	9
	P3	SEMI	top	12	1	9
	P4	SEMI	bot.	19	[2, 7]	11
	P5	SEMI	top	7	1	4
	P6	SEMI	top	15	1	4
	P7	SEMI	bot.	19	[2, 5]	9
	P8	FSO	bot.	19	[4, 5]	8
S3	ND	–	–	0	1	70

Notes: ND = Noble Denton; SEMI = Semi-submersible; FSO = floating storage and offloading vessel; FPSO = floating production, storage and offloading vessel; bot. = bottom; instal. = installation chain; C = Corrosion level.

with retrieved chain segments and one with new, uncorroded specimens. The first subset, here called subset S1, comprises 19 results of tests on retrieved specimens that were conducted at the Norwegian University of Science and Technology (NTNU). Subset S2 consists of 61 tests of retrieved specimens conducted by Det Norske Veritas-Germanischer Lloyd (DNV-GL), which are partially reported in [7,11,12]. Subset S3 consists of 70 test results of new, uncorroded chains by Noble Denton [19,20]. Note that subset S3 data were used to develop the design S–N curves in API RP 2SK [4] and DNVGL-OS-E301 [5].

2.1. Service life of the chains

The considered chain specimens were either new, i.e., subset S3, or retrieved after spending between 5 to 20 years in service, i.e., subsets S1 and S2. The distribution of the time in service of the tested specimens is shown in Fig. 2 and the range of values per platform and subset is shown in Table 1. The data set contains data from 8 different platforms, which are located either in the North Sea or in the Norwegian Sea. Note that we use the term platform to refer to any floating offshore unit. In the considered data set, platforms are of three types, namely semi-submersibles (SEMI), floating storage and offloading vessels (FSO) or floating production, storage and offloading vessels (FPSO). Minimum 6 and maximum 19 independent tests have been conducted for chain segments belonging to the same platform. Specimens from the same platform may have been in service for a different number of years and sometimes differ in mechanical properties, such as diameter, grade, and minimum breaking load (MBL). Specimens were retrieved from several locations of the mooring systems, namely the top section, the installation section and the bottom section, see Fig. 1. Note that the top section includes the splash zone and the turret, and the bottom section includes chain lengths below and above mudline.

The corrosion condition of the retrieved chain segments was visually assessed by a scientific researcher with 30 years of experience in material science and corrosion. The corrosion condition is measured by the corrosion level, which is an assigned integer between 1 (no corrosion) and seven (severe corrosion). The corrosion level assignment is based on quantitative and qualitative information and is meant as a synthesis of aspects of the corrosion condition that are likely to have an impact on fatigue resistance.

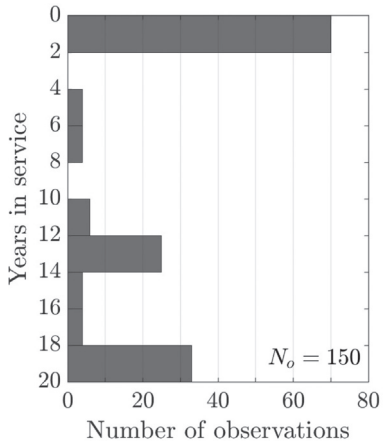

Fig. 2. Distribution of the years in service of the chains in the data set, including all $N_o = 150$ tested specimens.

The reference used for describing the seven corrosion levels, see Table 2, was derived to be representative of the corrosion condition of the retrieved chains. All the assignments were conducted by a single person to avoid biases in judgement. The assignment was conducted after visual inspection and no detailed measurement of pit depth took place. Links with corrosion levels 2, 4 and 7 are shown in Fig. 3. The ranges of corrosion levels of the specimens of the data set are shown in Table 1.

2.2. Mechanical properties

The considered specimens were produced following the required minimum mechanical properties in DNVGL-OS-E302 [21], which are given depending on grade. The actual mechanical properties of the specimens are typically well over the minimum requirements. The mechanical properties of the uncorroded steel of the links were provided by the manufacturers, see Table 3. The ratio between the measured average yield strength and tensile strength are also shown in Table 3. It can be seen that the measured yield strengths are quite above the minimum requirements in DNVGL-OS-E302, i.e., in the order of 50% over them in average. The measured tensile strengths differ less from the minimum requirements, being around 10% over them in average.

In addition, mechanical testing conducted at NTNU for the R4 material of subset S1, see Table 4. The cyclic material properties are not investigated in the current study. The reader can refer to [22] for the cyclic properties of corroded links that are similar to the considered ones.

2.3. Test setup

The main settings of the experimental setups are summarised in Table 5. The test rig used for subset S1 is shown in Fig. 4. It consists of a load frame with a 280 t servo hydraulic actuator placed at the top, and a load cell at the bottom. An Instron 8800

Table 2
Description of the seven corrosion levels used to characterise the corrosion condition of the specimens.

Level, C	Description
1	New chain; may be subject to mild uniform corrosion
2	Some scattered pitting, with pits less than 1 mm deep
3	Larger areas affected than level 2, with pit depths ca. 1 mm
4	Large area affected by pitting, with pit depths ca. 1-3 mm; crown area affected by pitting
5	Severe and widespread pitting, with pit depths up to 4 mm
6	Severe and widespread pitting, with pit depths up to 6 mm
7	Severe and widespread pitting, with heavily attacked crown; sharp pits, most being 3 to 6 mm deep, and some are even larger

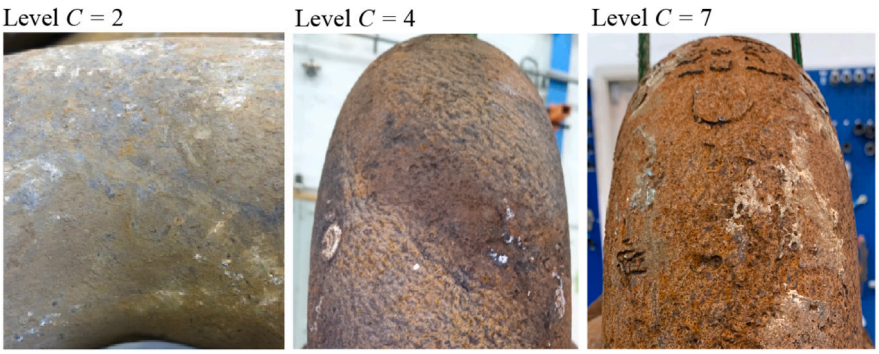

Fig. 3. Examples of links with different corrosion levels.

Table 3
Mechanical properties of the chain specimens in the data set. Values in square brackets correspond to [min, max] of the property.

	Subset S1	Subset S2	Subset S3
Nominal diameter [mm]	114	[114, 145]	76
Grade	R4	R3 & R4	R3 & R4
Yield strength[a] [MPa]	870	R3: 620; R4: 827	R3: 620; R4: 890
Yield strength[a]/R_e	1.47	R3: 1.51; R4: 1.43	R3: 1.51; R4: 1.53
Tensile strength[a] [MPa]	954	R3: 741; R4: 931	R3: 740; R4: 980
Tensile strength[a]/R_m	1.08	R3: 1.07; R4: 1.08	R3: 1.07; R4: 1.14

[a]Mean value from mechanical testing of few specimens.
Notes: R_e = minimum yield strength [21]; R_m = minimum tensile strength [21].

Table 4
Mechanical properties of the R4 material of subset S1 tested at NTNU, compared to the minimum requirements in DNVGL-OS-E302 [21].

	Elongation A_6	Reduction of of area Z	Charpy V-notch energy at −20 °C	
			Average of 3	Minimum
Test data	19%	71%	179 J	177 J
Required	12%	50%	50 J	38 J

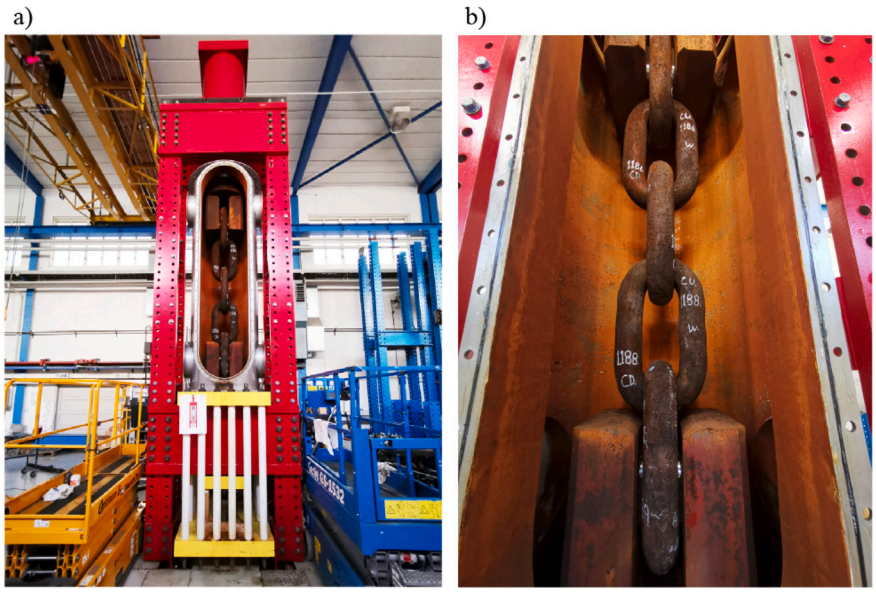

Fig. 4. (a) Test rig with 280 t load capacity used for subset S1, with a five-link specimen in position. During testing, a front panel is attached to seal the test chamber, which is subsequently filled with salt water. (b) Close-up of the five-link specimen in position inside the test chamber.

console was used to control and monitor the actuator load. The corrosion system consists of a stainless-steel cylindrical chamber, which can be sealed with a steel front plate. The inside of the chamber is painted to avoid rust contamination. The tests of subset S2 employed two different test rigs with capacities of 450 t and 750 t. The setups of these two rigs are similar to the one just described. Tests of subset S3 were conducted several decades ago, and the capacity of the rig is unknown to the authors. The rig employed for these tests had a horizontal layout in contrast to the vertical layout of the rigs of subsets S1 and S2. Nevertheless, this detail is not expected to have any significant effect on the results since these tests were conducted with high mean tension.

During testing, the segments were submerged in synthetic seawater containing 3.5% w/w of sodium chloride (NaCl), which was circulated by means of a pump. Even though corrosion degradation is not expected to significantly worsen during testing, the experiments are conducted in salted water since the medium may potentially affect crack growth development [23]. The salt content was monitored, and it remained stable throughout testing. Additionally, the pH and water temperature were monitored to follow the values in Table 5.

The frequency of the tests was set to be higher than the typical wave frequency in the North Sea, which is in the order of 0.17 Hz, see Table 5. Similar frequencies were employed for subsets S1 and S2, while subset S3 employed slightly higher frequencies. This frequency was chosen to reduce testing time, since it takes around 23 days to test one million cycles at 0.5 Hz. The effect of frequency

Table 5
Characteristics of the fatigue test setup. Values in square brackets correspond to [min, max] of the property.

	Subset S1	Subset S2 [7]	Subset S3 [19,20]
Test rig capacity	280 t	450 t and 750 t	Unknown
Number of links	3 and 5	5 and 6	5[a]
Temperature	[20, 23] °C	[19, 27] °C	[6, 9] °C
Frequency	0.5 Hz	[0.3, 0.5] Hz	[0.2, 0.7] Hz
pH	7	[6.5, 8.1]	[8, 8.2]

[a]Tests were conducted up to third-link failure.

on corrosion-fatigue crack growth of mooring chain steel in seawater was investigated by Zhang et al. [24] for grades R3, R4 and R5. The results from this study indicate a negligible difference in fatigue crack growth between 0.17 Hz and 0.5 Hz. A similar study by Hudak et al. [25] performed on high strength riser steels arrived at a similar conclusion. Based on these investigations, it is assumed that frequency effects can be neglected for the current data set.

Tests were conducted for specimens with different number of links, see Table 5. The more links are contained in one specimen, the sooner it is expected to fail for fatigue, due to the serial nature of the specimens. Therefore, the number of links is a statistically relevant parameter of the tests. Nevertheless, the effect of the number of links is not considered in the current study. The implications of this assumption are discussed in Section 7. It should be noticed that the S3 tests were conducted up to third-link failure, as opposed to the tests of subsets S1 and S2. Third-link failure implies that after failure of a link, the link was replaced by a Kenter link (as specified in [26]) and the test was continued, repeating this approach twice [20]. Testing a five-link chain up to third-link failure is somewhat similar to testing a three-link chain. Thus, this particularity is associated with similar limitations as those associated with neglecting the effect of number of links.

The contact area of each bolt was fitted to the curvature of each link to maximise the contact area. This was done to reduce stresses in the contact area between the link and the test rig, thereby reducing the probability of failure at these locations. Termination of the test was based on the actuator stroke monitoring. The test was set to stop after a pre-set target elongation of the test segment was reached. The target elongation, which is associated with through-thickness fracture, was based on the position of the actuator piston and was set to 10 mm, in addition to the elongation caused by the maximum load of the test.

2.4. Fatigue test inputs

The tests were conducted for various stress range values and for one or more mean stress levels. The experimental design of these two variables is shown in Fig. 5 and their scope is summarised in Table 6. Note that the majority (76%) of tests of retrieved specimens were conducted with a mean stress in the range 10% to 18% of MBL. In addition, the stress ratio R is shown in the table for direct comparison with the literature. The stress ratio is defined as

$$R = \frac{\sigma_{min}}{\sigma_{max}} = 1 - \frac{\Delta S}{\sigma_m + \Delta S/2} \tag{2}$$

with σ_{min} and σ_{max} being the minimum and maximum nominal stresses during testing and σ_m being the mean nominal stress.

3. Experimental results

The main outcome of the fatigue tests is the number of cycles to failure. The relation between the obtained cycles to failure and the applied stress ranges is plotted in log–log scale in Fig. 6. Furthermore, the locations of the observed fatigue failures are reported hereafter.

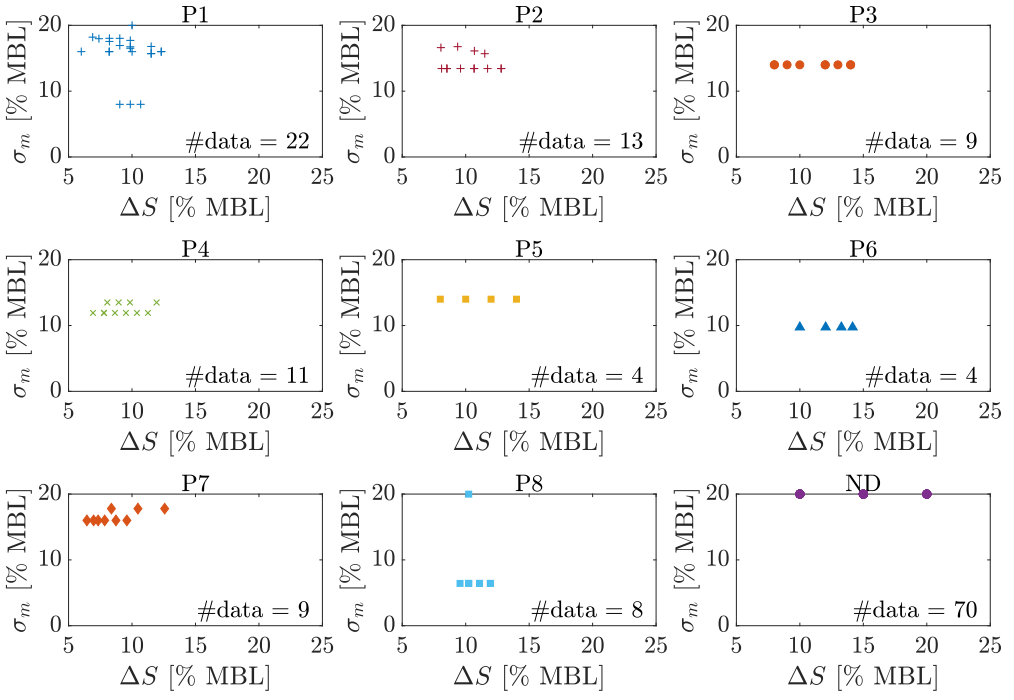

Fig. 5. Nominal mean stress and stress range input of the fatigue tests expressed.

Table 6
Range of values of the nominal mean stress and stress range input of the fatigue tests. Values in square brackets correspond to [min, max] of the variable.

Subset	Platform	Mean stress σ_m [MPa]	[% MBL]	Stress range ΔS [MPa]	[% MBL]	R [–]
S1	P1	[96, 110]	[15.7, 18.2]	[42, 70]	[6.9, 11.5]	[0.2, 0.7]
	P2	[97, 101]	[15.7, 16.7]	[49, 85]	[8.0, 14.0]	[0.4, 0.6]
S2	P1	[96, 122]	[15.7, 20]	[37, 75]	[6.0, 12.3]	[0.4, 0.7]
	P2	63	13.4	[38, 60]	[8.1, 12.8]	[0.4, 0.5]
	P3	80	14.0	[46, 80]	[8.0, 14.0]	[0.3, 0.6]
	P4	[69, 80]	[11.9, 13.5]	[40, 71]	[6.9, 11.9]	[0.4, 0.5]
	P5	[80, 81]	14.0	[46, 81]	[8.0, 14.0]	[0.3, 0.6]
	P6	55	9.7	[57, 80]	[10.0, 14.2]	[0.2, 0.3]
	P7	[92, 100]	[16.0, 17.8]	[37, 70]	[6.4, 12.6]	[0.5, 0.7]
	P8	[38, 117]	[6.4, 20.0]	[56, 70]	[9.6, 11.9]	[0.1, 0.6]
S3	ND	[108, 132]	20.0	[54, 132]	[10.0, 20.0]	[0.3, 0.6]

Notes: ND = Noble Denton; R = stress ratio.

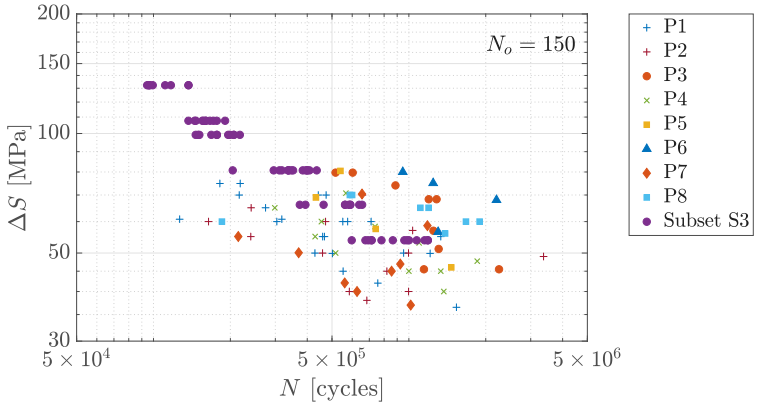

Fig. 6. Raw S–N data plotted in log–log scale, differentiating according to platform (P1–P8) and including new, uncorroded chain links. All $N_o = 150$ data points are included.

Fatigue failure of chain links tends to occur at one of the four fatigue hot spots: crown, K_t point, weld or straight areas. The K_t point is the intersection between the straight and bent parts of a link [27]. The different fatigue failure hot spots are illustrated in Fig. 7. The frequency of observed fractures at the hot spots are reported in Fig. 8 for the tested retrieved chain specimens (subsets S1 and S2). The great majority of failures occurred at the crown location, with the remaining failures happening at the K_t point and straight/weld parts. The frequency of the fracture locations is also presented in Table 7, which distinguishes between the three subsets. Observed frequencies of subsets S1 and S2 are comparable, although a higher frequency of failures at the straight part is reported for subset S1. Nevertheless, this difference may be accounted for by the fact that subset S1 comprises only 19 observations. What is more noticeable is that the observed frequencies for corroded specimens significantly differ from those observed for new, uncorroded chains (subset S3). Fracture of these specimens is characterised by a much larger proportion of failures in the K_t point

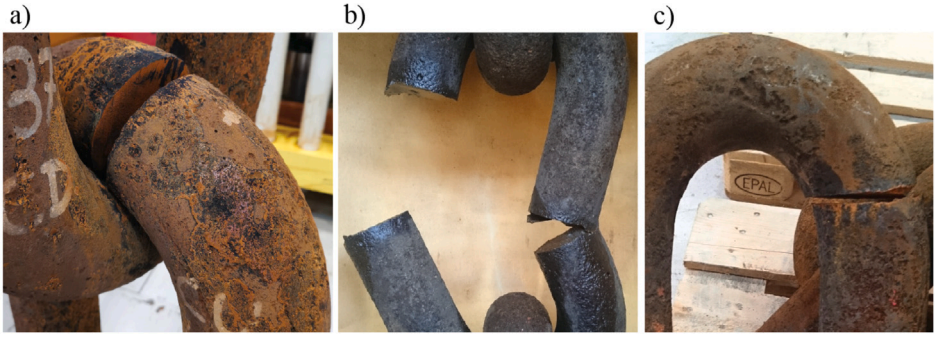

Fig. 7. Example of fracture locations after tension–tension fatigue testing: (a) crown failure; (b) Straight/weld failure; (c) K_t point failure.

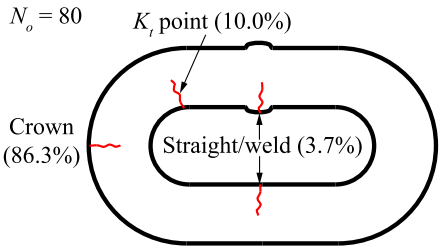

Fig. 8. Obtained frequency of fracture locations from the $N_o = 80$ fatigue testing results of retrieved corroded chains.

Table 7
Comparison of the frequency of the fracture locations between the three subsets S1, S2 and S3.

Location	Subset S1	Subset S2	Subset S3
Crown	84.2%	86.9%	34.0%
K_t point	5.3%	11.5%	52.0%
Straight/weld	10.5%	1.6%	14.0%

and the straight and weld areas, and a significantly lower proportion at the crown area. The fact that a horizontal test machine was employed for subset S3 is not likely to be the explanation for the difference in the frequencies of the failure locations. This assertion is supported by evidence from other horizontal testing campaigns of corroded specimens by Ma et al. [28], where five out of five link failures were observed at the crown. The large difference between the results of new and corroded specimens may be explained by two factors. First, used links present a larger wear at the crown, which leads to a reduced cross section. Second, finite element investigations by Zarandi et al. [27] indicate that pits at the crown are the most critical pits for fatigue crack initiation.

4. Data analysis methodology

4.1. Hierarchical structure of the data

Full-scale fatigue test data are typically scarce and different subpopulations are often combined in the development of S–N curves. This is the for the considered data set. As described in Section 2, the links were retrieved from several offshore platforms and differ from each other according to relevant features. Furthermore, the data set has been obtained from fatigue testing of chain links at several laboratories. Hierarchical models can be employed to address data belonging to different subpopulations in a consistent manner. The theoretical background of hierarchical models in the context of regression analysis is well documented in [29]. Based on the above considerations, it is clear that the data do not come from one homogeneous population. If the hierarchical character of the data is ignored, two extreme alternatives of analysis are:

(a) **No-pooling**. That is, to estimate separate models for each group or subpopulation. This means that different S–N curves can be fitted for each subpopulation by only considering the data belonging to them. Considering that the number of tests per subpopulation is very limited, this alternative leads to models with high statistical uncertainty. The excess of statistical uncertainty leads to over-fitting the data within each subpopulation. In other words, differences among subpopulations would be overstated and the inferred models would likely appear more different among each other than they would be if more data were available. This is due to the fact that the data shares important features across the different subpopulations. Therefore, isolating them in distinct subpopulations and analysing them separately results in a non-efficient use of available information.
(b) **Complete-pooling**. That is, to combine all data from different subpopulations and fit a single model. This analysis excludes categorical predictors from the model, which will lead to biases in the obtained model. This means that specific knowledge that could be learnt from the different subpopulations is averaged out and thereby partially lost.

The use of hierarchical models takes advantage of the complete data set while using subpopulation-specific information. In this study, we use a linear mixed-effects model to address the hierarchical structure of the data. A brief overview of the theory of linear mixed-effects models and its application to the modelling of the considered data set are presented hereafter.

4.2. Linear mixed-effects regression analysis

Random-effects models were proposed by Laird and Ware [30]. Linear mixed-effects models (LMEM) are a sub-type of the random-effects models. The principles of linear mixed-effects regression analysis are briefly presented in the following. A data set with N_o observations is considered. The data set is understood as composed of J disjoint subpopulations. Each subpopulation contains $n_{o,j}$ observations, so that

$$\sum_{j=1}^{J} n_{o,j} = N_o. \tag{3}$$

Generally speaking, an LMEM of the data is composed of the superposition of a fixed-effects model and a random-effects model, and is mathematically represented by the following equation:

$$\mathbf{y} = \mathbf{X}\boldsymbol{\beta} + \mathbf{Z}\boldsymbol{\gamma} + \boldsymbol{\varepsilon}, \tag{4}$$

where $\mathbf{y}$ is the $N_o \times 1$ vector of uncontrolled response variables; $\boldsymbol{\beta}$ is the $p \times 1$ vector of fixed-effects coefficients, with p being the number of predictors, including the intercept; $\mathbf{X}$ is the $N_o \times p$ design matrix of the p predictor controlled variables, with the first column being a column of ones; $\mathbf{Z}$ is the $N_o \times q \cdot J$ design matrix of the q random-effects, which maps the random-effects with the subpopulation with which they are associated; $\boldsymbol{\gamma}$ is the $q \cdot J \times 1$ vector of random-effect coefficients; and $\boldsymbol{\varepsilon}$ is the $N_o \times 1$ vector of residuals.

The fixed-effects coefficients $\boldsymbol{\beta}$ are common to all subpopulations and are computed using the complete data set, while the random-effects coefficients $\boldsymbol{\gamma}_j$ only use observations in subpopulation j. The part of the LMEM associated with subpopulation j is

$$\mathbf{y}_j = \mathbf{X}_j\boldsymbol{\beta} + \mathbf{Z}_j\boldsymbol{\gamma}_j + \boldsymbol{\varepsilon}_j. \tag{5}$$

Let $N(\boldsymbol{\mu}, \boldsymbol{\Sigma})$ denote, generally, the multi-variate normal distribution with mean vector $\boldsymbol{\mu}$ and covariance matrix $\boldsymbol{\Sigma}$. According to the central limit theorem, the distribution of the vector of random-effects coefficients of a given subpopulation is assumed to be $\boldsymbol{\gamma}_j \sim N(0, \mathbf{D})$. Similarly, and assuming statistical independence among responses $\mathbf{y}_j$ conditional on the model parameters, the distribution of the residuals is $\boldsymbol{\varepsilon}_j \sim N(0, \sigma^2\mathbf{I})$, where $\mathbf{I}$ is the $N_0 \times N_0$ identity matrix. It then follows that the marginal distribution of the response is $\mathbf{y}_j \sim N(\mathbf{X}_j\boldsymbol{\beta}, \mathbf{Z}_j\mathbf{D}\mathbf{Z}_j^{\mathrm{T}} + \sigma^2\mathbf{I})$ [30]. Note that the term $\mathbf{Z}_j\mathbf{D}\mathbf{Z}_j^{\mathrm{T}}$ introduces statistical dependence among observations from the same subpopulation.

For the particular case of having $p = 1$ predictor variables, with fixed slope β_1 and fitted intercept β_0, and $q = 1$ random-effects, i.e., only random intercepts, the model simplifies to

$$\mathbf{y} = \beta_0 + \beta_1\mathbf{x} + \boldsymbol{\gamma}_0 + \boldsymbol{\varepsilon}, \tag{6}$$

where $\boldsymbol{\gamma}_0$ is the $J \times 1$ random intercept vector, with distribution $\boldsymbol{\gamma}_{0,j} \sim N(0, \tau_0^2)$.

In this case, the correlation among two observations i and l of the same subpopulation j is

$$\mathrm{Corr}[y_{j,i}; y_{j,l}] = \frac{\mathrm{Cov}[y_{j,i}; y_{j,l}]}{\sqrt{\mathrm{Var}[y_{j,i}]\mathrm{Var}[y_{j,l}]}} = \frac{\tau_0^2}{\tau_0^2 + \sigma^2} \quad \text{with } i \neq l, \tag{7}$$

with $\mathrm{Corr}[\cdot;\cdot]$, $\mathrm{Cov}[\cdot;\cdot]$ and $\mathrm{Var}[\cdot]$ being the correlation, covariance and variance operators, respectively. When using the best estimates of τ_0 and σ, here denoted τ_0^* and σ^* respectively, the value that results from this equation is typically known as the intra-class correlation (ICC). Thus, the LMEM interprets the hierarchy in the data as a linear correlation among data from the same subpopulation.

4.3. Process behind the data

The observed fatigue life from the experiments is the result of complex stochastic phenomena that are influenced by many variables. Fig. 9 shows a simplified representation of the causal relation between influencing variables and fatigue life. This type of representation is a so-called causal network [31], which allows to clearly state the underlying assumptions of the data analysis. In a causal network, the circular nodes represent variables, and the arcs represent causal relationships, with the arrows pointing from cause to effect.

In the proposed causal model, the obtained number of cycles to failure N of a chain segment is directly affected by several non-controlled and controlled variables. The non-controlled variables are the number of years in service T_S, the corrosion condition C, and a set of (unobserved) additional variables M_1. The controlled variables are the applied stresses during fatigue testing, which include the nominal mean stress σ_m and the nominal stress range ΔS. Because these variables are controlled during testing, they are independent of the platform. Following the same logic, the non-controlled variables T_S, C and M_1 do depend on the platform P from where the chain segments have been sampled. Note that P affects C through a set of mediator variables M_2. M_1 and M_2 are two disjoint sets. The set M_1 includes all variables that affect fatigue life and do not affect the corrosion condition, such as initial defects, the residual stresses, and the experienced stresses during time in service. The set M_2 includes all variables that affect the corrosion condition but do not directly affect fatigue life, such as temperature, dissolved oxygen and pH [10,32].

A variable that simultaneously affects the corrosion condition and the fatigue life may result in a confounding bias, meaning that if this variable is not properly controlled for, the statistical analysis may result in a larger estimation of the statistical dependence among corrosion and fatigue life than can be accounted for by the actual causal effect. Thus, these variables are to be explicitly represented in the causal diagram. In the model, N and C are both dependent on the time in service T_S, because this variable simultaneously increases the corrosion condition and the expected accumulated fatigue damage. Nevertheless, time in service affects corrosion condition and fatigue life in fundamentally different ways. The development of pitting corrosion in time is a concave functional relationship [10], implying that its development decelerates with time, whereas crack growth is a convex function [24]. The latter implies that mooring chains are not expected to accumulate significant fatigue damage during most of their service life, particularly considering that they are typically designed with large fatigue safety margins [12]. Furthermore, the tested specimens did not present any visible initial fatigue cracks. The same observation was reported in Gabrielsen et al. [11], which reports that fracture of the specimens considered in that investigation took place in the base material, with no prior identification of cracks.

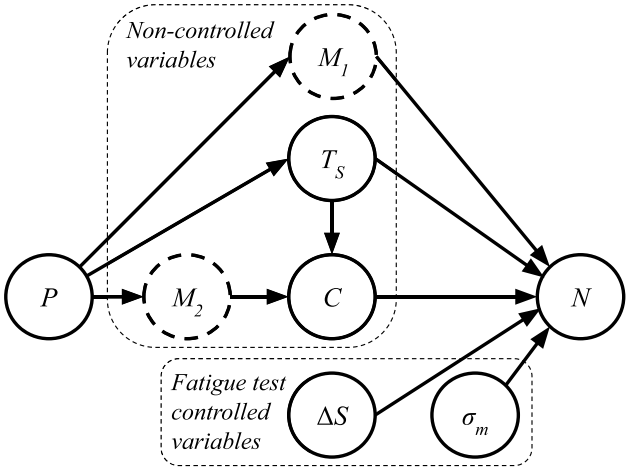

Fig. 9. Causal diagram to study the effect of corrosion on fatigue life. The following nomenclature is used: P = platform; N = fatigue life; C = corrosion condition; T_S = time in service; ΔS = nominal stress range; σ_m = nominal mean stress; M_1 = unobserved set 1 of mediators; and M_2 = unobserved set 2 of mediators.

In addition, corrosion condition leads to a change in the fatigue failure location, as shown in Table 7. Thus, most of the fatigue damage accumulated during the initial years of service is not occurring at the most likely failure location of a corroded link, which is the crown. Due to these considerations, the confounding effect caused by the time in service is expected to be low and therefore, it is neglected for simplicity.

Furthermore, the following additional assumptions are implicit in the model. For a given stress range, the effect of diameter on fatigue life is not significant [33]. Similarly, the effect of grade has little influence on fatigue life, see [33,34], and is consequently neglected in the model for simplicity.

According to these considerations, we conclude that dividing the data set into subpopulations based on platform allows us to deconfound the effect of corrosion condition on fatigue life. Lastly, the controlled variables of the fatigue test are regarded. The scope of the applied nominal mean stresses and stress ranges is shown in Table 6 and Fig. 5. For any given platform, the scope of applied nominal stress ranges is sufficiently representative to assess the effect of this variable. Specially, considering that it is common practice to assume that this effect is known and represented by a value of $m = 3$ in Eq. (1). However, the same cannot be argued for the scope of applied nominal mean stresses. On the contrary, the variability of the applied mean stresses is rather low or even non-existent within most platforms. This is the case for the data of platforms P3 to P8 and the Noble Denton data. Thus, mainly the data from platforms P1 and P2 are valuable to empirically assess the mean stress effect. Since the focus of the current study is on the assessment of the corrosion effect, all considered data should be regarded to have a representative set of specimens showing a wide range of corrosion levels. Thus, it is concluded that the considered data set is not suitable for simultaneously assessing the corrosion and mean stress effects. Even though the mean stress effect cannot be properly assessed empirically using the considered data set, alternative methods exist in the literature to take it into account. In the following subsection, the application of some of the available mean stress correction methods are discussed in the context of the current study.

4.4. Consideration of mean stress effect with correction models

The effect of the applied mean stresses during testing should be considered in the analysis to abstract the effect of the corrosion condition from the data. Unfortunately, the experimental designs of the three considered data sets is not suitable to assess the mean stress effect. Alternatively, one can use available mean stress correction models to deterministically take this effect into account. As an example, Fernandez et al. [14] use three well known mean stress correction models, namely Goodman, Gerber and Smith-Watson-Topper (SWT), to assess the effect of mean stress on the intercept of the S–N curves. In the current study, we consider the same three correction models, which are presented in Table 8 as per the formulation in [35].

According to these correction models, an equivalent stress range can be computed as a function of the applied mean stress and stress range, and in the case of the Goodman and Gerber models, also the ultimate tensile strength of the steel. The equivalent stress range is the completely reversed stress range that leads to the same damage as the pair of stress range and mean stress. The completely reversed stress range is associated with a stress ratio $R = -1$, or equivalently, $\sigma_m = 0$.

By applying the different correction models to the data, one can estimate how sensitive is the estimated corrosion effect with respect to the consideration of the mean stress effect for the current data set. Thus, these models are used in Section 5 to assess the influence of the mean stress effect on the inferred fatigue resistance models.

Table 8
Considered mean stress correction models. ΔS_{eq} is the equivalent fully reversed stress range.

Name	Model
Goodman	$\Delta S_{eq} = \frac{\Delta S}{1 - \frac{\sigma_m}{\sigma_u}}$
Gerber	$\Delta S_{eq} = \frac{\Delta S}{1 - (\frac{\sigma_m}{\sigma_u})^2}$
SWT	$\Delta S_{eq} = \sqrt{\Delta S(2\sigma_m + \Delta S)}$

Note: σ_u = ultimate tensile strength of the steel.

Table 9
Hierarchically structured data set. Values in square brackets correspond to [min, max] of the property.

Subpopulation	Platform	$N_{o,j}$	Corrosion level	Years in service
G1	P1	19	[2, 6]	[10, 20]
G2	P2	15	[1, 7]	[5, 18]
G3	P3	9	1	12
G4	P4	11	[2, 7]	[12, 19]
G5	P5	4	1	7
G6	P6	4	1	15
G7	P7	9	[2, 5]	[16, 19]
G8	P8	8	[5, 7]	[19, 20]
G9	Noble Denton [20]	70	1	0

4.5. Linear mixed-effects model of the fatigue data

According to the considerations in Section 4.3, the data set is divided into $J = 9$ subpopulations, see Table 9. The generic LMEM in Eq. (4) is then adapted to the current case:

$$\log_{10}(N_{i,j}) = -m \cdot \log_{10}(\Delta S_{i,j}) + \beta_2 \cdot \log_{10}(C_{i,j}) + \log_{10}(k) + \gamma_{0,i,j} + \epsilon_{i,j}, \tag{8}$$

where $i = 1, 2, \ldots, N_{o,j}$ refers to a data point of subpopulation $j = 1, 2, \ldots, J$. The following substitutions are made:

- $y_{i,j} = \log_{10}(N_{i,j})$;
- $\mathbf{x}_{i,j} = [\log_{10}(\Delta S_{i,j}), \log_{10}(C_{i,j})]$;
- $\boldsymbol{\beta} = [\beta_0 = \log_{10}(k), \beta_1 = -m, \beta_2]$.

The stress range effect is assumed to be fixed to $m = 3$, according to industry convention [5,16]. Consequently, the model has the following degrees of freedom: three regression parameters for the fixed-effects model $(k, \beta_2, \varepsilon)$ and $J = 9$ random intercepts $\boldsymbol{\gamma} = \{\gamma_1, \gamma_2, \ldots, \gamma_J\}$. Note that the mean stress correction models in Table 8 can be easily implemented by substituting $\Delta S_{i,j}$ with the corresponding equivalent stress range $\Delta S_{eq,i,j}$.

5. Results of data analysis

In this section, the data set is used to infer a fatigue resistance model of the form of Eq. (8). First, the regression analysis is conducted by neglecting the mean stress effect. The obtained model is referred to as the "reference model" in the following. The model parameters are computed using the Statistics and Machine Learning Toolbox of Matlab© [36], which employs a two-step integration using restricted maximum likelihood and maximum likelihood methods.

The inferred parameters of the reference model are shown in Table 10. The standard deviation of the model residuals results in $\sqrt{\tau_0^2 + \sigma_\varepsilon^2} = 0.268$. The obtained ICC indicates that the data belonging to a given platform are moderately correlated to each other. The mean S–N curves of the different subpopulations are estimated using their associated random-effects terms and the average corrosion level of their specimens. These curves are plotted in Fig. 10, including the mean fixed-effects curve for reference.

According to the extended S–N model, the relation between the number of cycles to failure (N_1 and N_2) associated with two different corrosion levels (C_1 and C_2) is given by

$$\frac{N_1}{N_2} = \left(\frac{C_1}{C_2}\right)^{\beta_2}. \tag{9}$$

If we regard the typical S–N relation in Eq. (1), differences in the number of cycles to failure are solely caused by differences in the stress range. Let A_1 and A_2 be the nominal cross-section areas associated with the stress ranges ΔS_1 and ΔS_2, respectively.

Table 10
Maximum likelihood estimation of the linear mixed-effects model parameters of the reference model, i.e., without accounting for mean stress effect. Units are in accordance with stresses in MPa.

Parameter	Type	Mean	Std. deviation
m	Deterministic	3	–
$\log_{10} k$	Normal	11.478	0.099
β_2	Normal	−0.802	0.125
σ_ε	Normal	0.165	0.0251
τ_0	Normal	0.211	0.0392
ICC	Deterministic	0.621	–

Notes: σ_ε = std. deviation of the model residuals; τ_0 = std. deviation of the random effects; ICC = Intra-class correlation.

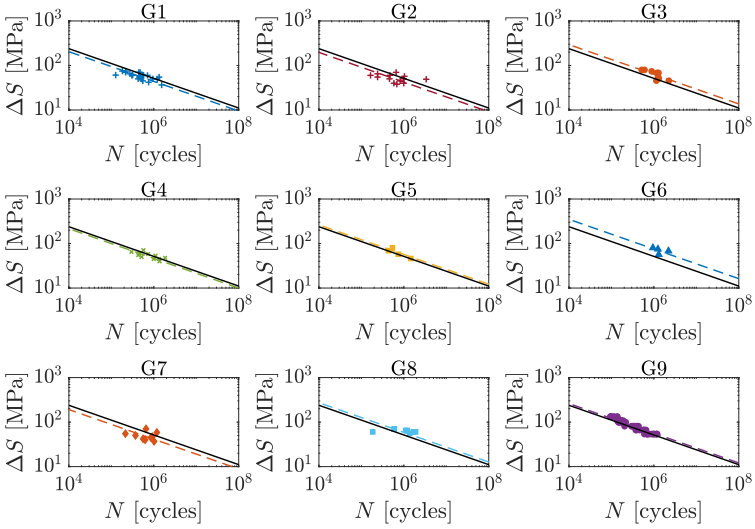

Fig. 10. Mean S–N curve for the different subpopulations. Additionally, the mean fixed-effects curve is plotted for reference in continuous black.

The nominal stress range of a chain link is inversely proportional to the cross-section area. Thus, from Eq. (1), we get that the ratio between N_1 and N_2 for constant nominal tension is

$$\frac{N_1}{N_2} = \left(\frac{A_1}{A_2}\right)^m. \tag{10}$$

Combining Eqs. (9) and (10) leads to:

$$\frac{A_1 - A_2}{A_1} = 1 - \left(\frac{C_2}{C_1}\right)^{\beta_2/m}, \tag{11}$$

which represents the reduction in cross section (from A_1 to A_2) that should be observed if the corrosion-effect would be simply attributed to uniform corrosion. Based on Eq. (11), it is deduced that an increase of the corrosion level from $C_1 = 1$ to $C_2 = 7$ would need to be explained by a reduction in cross-section area of approximately $1 - 7^{-0.802/3} \approx 40\%$. This estimate corresponds to a reduction of ca. 23% of the chain diameter. Since the observed reduction of the diameters for the tested specimens with $C = 7$ is significantly lower than that, it is concluded that the fatigue-corrosion effect is more complex in nature and leads to significantly lower fatigue lives that what can be accounted for by uniform corrosion. Thus, the corrosion condition should be implicitly included as an input of the S–N curve to consider this effect.

To address the effect of mean stress on the inferred fatigue resistance models, the mean value estimates of the parameters of the reference model and of the three considered mean stress corrected models are shown in Table 11. The inferred parameters are independent of the stress ratio R, with the exception of the intercept $\log_{10} k$. The corrosion-effect parameter β_2 is not significantly affected by the consideration of the mean stress effect for the current data set. In particular, the Gerber corrected model leads to the lowest difference in the estimation of this parameter. In general, applying a mean stress correction model leads to a reduced uncertainty of the inferred model. The largest reduction is achieved with the SWT correction, which leads to a standard deviation of the model residuals of $\sqrt{\tau_0^2 + \sigma_\varepsilon^2} = 0.214$, which is 20% lower than for the reference model. This result is in line with the conclusions in Fernandez et al. [14], which indicate that the SWT provides the best representation of the effect among the three correction models.

Table 11
Comparison of the mean value of the inferred model parameters between the reference model and the mean stress corrected models. Units are in accordance with stresses in MPa.

Parameter	Reference model	Goodman	Gerber	SWT
$\log_{10} k$	11.478	11.614	11.492	12.342
β_2	−0.802	−0.837	−0.808	−0.882
σ_ϵ	0.165	0.158	0.164	0.139
τ_0	0.211	0.192	0.208	0.163
ICC	0.621	0.595	0.617	0.579

Notes: σ_ϵ = std. deviation of the model residuals; τ_0 = std. deviation of the random effects; ICC = Intra-class correlation.

The main implications of the mean stress effect are the reduction of fatigue resistance for increasing mean stress. The intercept of the typical two-dimensional S–N curve is plotted in Fig. 11 as a function of the stress ratio. This intercept can be easily computed by adding the corrosion effect to $\log_{10} k$, i.e., $\log_{10} k + \beta_2 \cdot C$. The SWT model is employed for these plots for illustration purposes and because it provides the largest reduction of model uncertainty among the considered mean stress correction models, see Table 11. Furthermore, the SWT model has the advantage of being independent from any material property. It can be observed that for values of R within the range of the data set, i.e., between 0.1 to 0.7 (see Table 6), the corrosion effect has a larger potential for reducing fatigue life than the mean stress effect.

6. Case study

In this section, the inferred extended S–N model is applied to computing the structural reliability of a mooring line segment. The cumulative probability of fatigue failure of a mooring line segment with a remaining service life of T years is denoted $P_{f,T}$. A mooring line segment is assumed to consist of a similar number of links to those of the specimens of the employed data set, i.e., between 3 and 5. A function g that limits the fatigue failure domain by $g \leq 0$ is introduced. $P_{f,T}$ results then from integrating the joint distribution of the involved random variables $\boldsymbol{X}$ over the failure domain, i.e.,

$$P_{f,T} = \Pr[g(\boldsymbol{x}; T) \leq 0]. \tag{12}$$

The Palmgren–Miner failure criterion is used to elaborate the limit state function g of the S–N fatigue resistance model:

$$g(\boldsymbol{x}; T) = \Delta - D(\boldsymbol{x}; T). \tag{13}$$

In this equation, $D(\boldsymbol{x}; T)$ is the damage accumulated during the period T and Δ is the uncertain Palmgren–Miner failure threshold, which is represented as a log-normal distributed random variable with mean 1 and coefficient of variation 0.3, according to JCSS [37].

Given that the average number of stress cycles in a year ν is known, $D(\boldsymbol{x}; T)$ can be approximated from the expected damage per cycle as

$$D(\boldsymbol{x}; T) = 1 = \sum_{i=1}^{\nu \cdot T} \Delta D_i \approx \nu \cdot T \cdot \mathbb{E}_T \left[\Delta D_i(\boldsymbol{x}) \right], \tag{14}$$

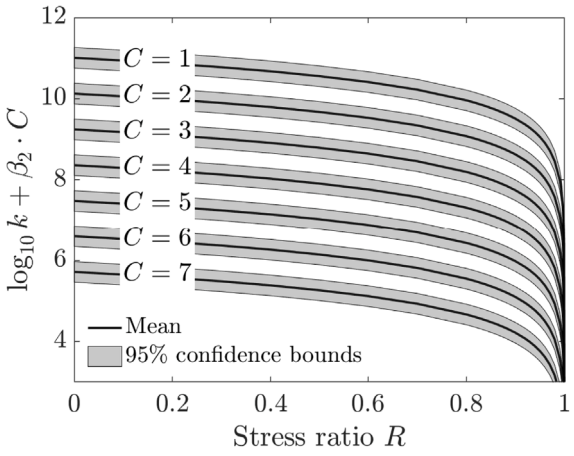

Fig. 11. Sum of the intercept $\log_{10} k$ and the corrosion effect $\beta_2 \cdot C$ of the SWT-corrected model as a function of the stress ratio R and for the different corrosion levels.

where ΔD_i is the increase in damage due to cycle i and $\mathbb{E}[\cdot]$ represents the expectation operator. The variable ν is assumed to be $5 \cdot 10^6$ cycles/year, which is typical for North Sea conditions [38].

The expected damage per fatigue cycle conditional on the corrosion level C follows from the model in Eq. (8):

$$\mathbb{E}_T\left[\Delta D_i|C\right] = \mathbb{E}\left[\frac{1}{N}\right] = \frac{1}{k \cdot 10^{\epsilon}} \cdot \mathbb{E}_T[\Delta S(t)^m] \cdot C^{-\beta_2}, \tag{15}$$

where $\Delta S(t)$ is the fatigue stress range process. Assuming that the cyclic stresses are dominated by the wave-induced loading, $\Delta S(t)$ is typically well represented by a Weibull distribution, with scale parameter k_w and shape parameter λ [39]. This process can then be reduced to an equivalent fatigue stress range ΔS_e that leads to the same expected fatigue life as the process, and which is given by

$$\Delta S_e = \mathbb{E}_T[\Delta S(t)^m]^{1/m} = k_w \cdot \Gamma\left(1 + \frac{m}{\lambda}\right)^{1/m}, \tag{16}$$

where $\Gamma(\cdot)$ is the complete gamma function. This equivalent fatigue stress ΔS_e is not to be confused with ΔS_{eq} in Table 8.

The expected damage per fatigue cycle can then be explicitly computed by substituting Eq. (16) into Eq. (15). The conditional limit state function is then given by substitution of Eqs. (14) and (15) into Eq. (13):

$$g(\boldsymbol{x}; T|C) = \Delta - \nu \cdot T \cdot \frac{1}{k \cdot 10^{\epsilon}} \cdot k_w \cdot \Gamma\left(1 + \frac{m}{\lambda}\right) \cdot C^{-\beta_2}. \tag{17}$$

Inserting Eq. (17) into Eq. (12) provides an expression for the probability of failure conditional on the corrosion level $P_{f,T|C}$. This expression can be solved by using e.g., the first order reliability method (FORM). The parameters of the fitted fatigue resistance model that are used in Eq. (17) are the ones of the reference model shown in Table 10. The rest of the involved random variables are summarised in Table 12. The parameter k_w of the Weibull distribution representing the fatigue stresses is calibrated so that the probability of failure of the uncorroded mooring line is 10^{-5} for a total design service life of 30 years. The coefficient of variation of k_w is taken as 0.22 after Moan and Song [40].

The conditional probability of failure $P_{f,T|C}$ is plotted as a function of the corrosion level and for different values of the remaining service life T in Fig. 12. The results are indicative for the estimation of the increase of the conditional probability of failure for increasing corrosion level. For instance, it can be seen that should the corrosion level stay constant in time, the 10-year cumulative probability of failure for $C = 4$ is more than 100 times higher than for $C = 2$.

The square of the FORM-sensitivity factors are plotted in Fig. 13. An intermediate but relatively severe corrosion level ($C = 5$) is chosen for the plot to show the sensitivity of the corrosion-effect parameter β_2. Choosing a lower or higher corrosion level results in, respectively, a higher or lower share of the sensitivity of the other parameters. Note that the differences in the sensitivity factors for other corrosion levels are not significant and are not shown for clarity. It is seen that the probability of failure is largely dominated by the model uncertainty ϵ and the parameter k_w of the fatigue stress distribution. Although the model uncertainty can be partially reduced by conducting additional experiments, this uncertainty is largely associated with the level of simplification implicit in the

Table 12
Probabilistic distribution of the involved variables.

Random variable	Type	Mean	Std. deviation
k_w [N/mm^2]	Log-normal	1.25	0.28
λ [–]	Deterministic	0.8	–
ν [cycles/year]	Deterministic	10^5	–

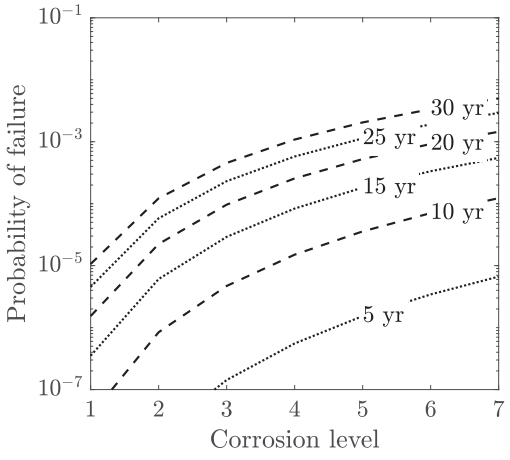

Fig. 12. Conditional probability of fatigue failure $P_{f,T|C}$ of a mooring line segment with a design service life of 30 years, as a function of the corrosion level C and for different values of the remaining service life T.

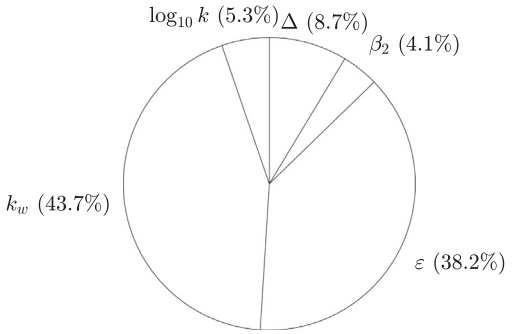

Fig. 13. FORM sensitivity factors for corrosion level 5 expressed as a percentage.

S–N representation of fatigue resistance. Therefore, significant savings can be achieved by conditioning the model on situation-specific data. Most of the uncertainty associated with k_w is aleatoric in nature and thus cannot be reduced. Nevertheless, the large sensitivity associated with this parameter indicates that efforts dedicated to improving the accuracy of the load modelling will have a significant impact in the estimation of the structural reliability.

7. Discussion

Fatigue test data were analysed to study the effect of the corrosion condition of mooring chains on their fatigue resistance. The results of the data analysis rely on the assumptions used to describe the relationship among the involved variables. A causal diagram has been proposed to explicitly display the assumptions employed to hierarchically organise the data. This can be used to study the validity of the proposed causal model in future studies. A linear mixed-effects model is implemented to efficiently use available information. The random-effects part of the model consists of the random-intercepts of the different subpopulations. No random slopes are considered, mainly because little variation of the corrosion level exists within a given subpopulation. Larger data sets that include larger variations of the corrosion condition could be used in future studies to validate the presented results and to improve their statistical significance.

The study shows that the effect of the corrosion condition on fatigue resistance is significant. Nevertheless, limited knowledge exists about which features of corrosion are more relevant to the prediction of fatigue resistance. In this article, the corrosion level C is used as an indicator of the corrosion condition. The corrosion level is a subjectively assigned number used to quantify the general severity of pitting corrosion, wear, and uniform corrosion. Thus, it is a synthesis of many factors that are hypothesised to be of relevance. Further studies should be conducted to investigate which features of corrosion have a higher impact on fatigue resistance. An objective indicator function could then be learned from these factors. The present results could be used as a reference for the development of the objective corrosion indicator. The objective indicator function could be used to assess the corrosion condition from collected in-situ information using, for instance, surface scanning technology.

The results of the reliability case study in Section 6 show that the corrosion effect has a significant impact on the reliability of a mooring segment conditional on the corrosion level. The level of detail of the analysis is guided by the level of detail of the representation of fatigue and corrosion, i.e., by the proposed extended S–N curve. It should be noted that corrosion deterioration is a time-dependent process. Hence, a time-evolution model of corrosion needs to be used to compute the unconditional reliability. Available models in the literature, see e.g. [10], suggest that the anaerobic growth of pit depths is very aggressive initially and slows down with time. According to this type of growth, chain segments that belong to nearby locations of a mooring line but that initially present different corrosion levels would tend to have more similar corrosion levels with time and likely spend most of their remaining lives with similar corrosion levels. Thus, we argue that the difference between the unconditional probabilities of failure of two segments of a line with different corrosion levels is lower than the difference between the conditional probabilities in Fig. 12.

Failure of a mooring chain occurs when any of its links fails. Thus, the number of links is statistically relevant to assess the structural reliability of mooring lines. In the present study, the effect of the number of links is not taken into account. This corresponds to assuming the different failure mechanisms of the tested specimens to be fully dependent, which is in line with the methods used in DNVGL-OS-E301 [5]. Some methods have been proposed to treat this effect based on order statistics and assuming full independence of the failure mechanisms [41]. In reality, the true effect will be in between the assumptions of dependence and independence. It is worth noticing that the dependence of the failure mechanisms is given by the dependence among material properties and load effects that affect fatigue resistance. Thus, dependence is expected to be significantly higher for chains subject to pitting corrosion than for new chains because this type of corrosion is shown to influence the location of fatigue failure and to reduce fatigue resistance. It is noted that the dependence assumption implicit in the current study and in DNVGL-OS-E301 [5] is however in contradiction with continuing the tests after the first failure is encountered, which is the case for the Noble Denton data of subset S3. It is recommended to conduct further studies to assess the true effect of the number of links. Nevertheless, it should be kept in mind that the uncertainty associated with not considering this effect is significantly lower than the inherent uncertainty of the fatigue phenomenon.

The effect of the number of links is of special relevance for applying the derived models for the assessment of long mooring lines, since the tested specimens contain a low number of links. The authors argue that this effect decays for increasing number of links. That is, for sufficiently long mooring lines, adding an additional link does not significantly increase their probability of failure. This is due to the fact that the probability of failure of the chain is dominated by few failure mechanisms. Further studies should be performed to validate this assumption.

Design standards for the design of mooring lines often neglect the mean stress effect [4,5]. This assumption is based on the presumption that failure occurs at welded connections, where there are large residual stresses [16]. As shown in the current experimental study, corroded links fail at the crown in most cases. Thus, the hypothesis used to neglect mean stress effects does not hold and further studies should be conducted to understand and quantify this phenomenon. In the present study, we use well known mean stress correction models, namely the Goodman, Gerber and SWT models, to account for the mean stress effect. We show that, for the regarded data set, the estimated corrosion effect is not very sensitive to which correction model is used or even if a correction model is used at all. This is of course not in contradiction with the fact that mean stress may have a significant impact on the fatigue resistance of corroded chains. Future research studies should aim at empirically assessing the mean stress effect for mooring chains, developing, and identifying the most appropriate models to assess this phenomenon and quantifying the uncertainty associated with the models.

8. Conclusions

Tension–tension fatigue test results of new and retrieved mooring chain segments were analysed to study the effect of the corrosion condition on fatigue resistance. The considered data set contains new as well as previously published data. The fatigue test setup and employed procedures were described. A hierarchical approach is proposed to analyse the data to maximise the use of available information. An extended S–N curve that includes a corrosion level indicator is developed using a linear mixed-effects model. The assessed effect of corrosion condition on fatigue resistance is significant. Well known mean stress correction models were used to assess how accounting for the mean stress effect affects the estimated corrosion effect. It was shown that the estimated corrosion effect is not significantly affected by mean stress correction. A numerical example is presented to illustrate the implications of the assessed fatigue-corrosion damage effect on the structural reliability of mooring lines. The results of the analysis can be used to inform integrity management and life-extension decisions of existing mooring systems and to enhance the design of new mooring chains.

Declaration of competing interest

The authors declare that they have no known competing financial interests or personal relationships that could have appeared to influence the work reported in this paper.

Acknowledgements

The authors would like to acknowledge the KPN Lifemoor project (RCN contract No: 280705) for providing the fatigue test data used in this article. In particular, the authors would like to acknowledge the insights provided by Øystein Gabrielsen and the assistance of Christian Frugone. Furthermore, the comments by Cody Owen are much appreciated.

References

[1] Fontaine E, Kilner A, Carra C, Washington D, Ma K, Phadke A, Laskowski D, Kusinski G, et al. Industry survey of past failures, pre-emptive replacements and reported degradations for mooring systems of floating production units. In: Offshore technology conference, no. OTC-25273-MS. Offshore Technology Conference; 2014.

[2] Gordon RB, Brown MG, Allen EM, et al. Mooring integrity management: a state-of-the-art review. In: Offshore technology conference, no. OTC-25134-MS. Offshore Technology Conference; 2014.

[3] ISO. Petroleum and natural gas industries - specific requirements for offshore structures — Part 7: Stationkeeping systems for floating offshore structures and mobile offshore units. Standard ISO 19901-7:2013, Geneva, Switzerland: International Organization for Standardization; 2013.

[4] API. Design and analysis of stationkeeping systems for floating structures, third edition. Recommended guide API RP 2SK, Washington, D.C, USA: API Publishing Services; 2015.

[5] DNV-GL. Position mooring. Offshore standard DNVGL-OS-E301, 2015.

[6] Pérez-Mora R, Palin-Luc T, Bathias C, C. Paris P. Very high cycle fatigue of a high strength steel under sea water corrosion: A strong corrosion and mechanical damage coupling. Int J Fatigue 2015;74:156–65. http://dx.doi.org/10.1016/j.ijfatigue.2015.01.004, URL http://www.sciencedirect.com/science/article/pii/S0142112315000067.

[7] Fredheim S, Reinholdtsen S, Håskoll L, Lie H. Corrosion fatigue testing of used, studless, offshore mooring chain. In: International conference on ocean, offshore and arctic engineering, no. OMAE2013-10609. American Society of Mechanical Engineers Digital Collection; 2013.

[8] Arredondo A, Fernández J, Silveira E, Arana JL. Corrosion fatigue behavior of mooring chain steel in seawater. In: International conference on ocean, offshore and arctic engineering, no. OMAE2016-54426. American Society of Mechanical Engineers Digital Collection; 2016.

[9] Morgantini M, MacKenzie D, Gorash Y, van Rijswick R. The effect of corrosive environment on fatigue life and on mean stress sensitivity factor. In: MATEC web of conferences, vol. 165. EDP Sciences; 2018, http://dx.doi.org/10.1051/matecconf/201816503001.

[10] Melchers RE. Pitting corrosion of mild steel in marine immersion environment—Part 1: Maximum pit depth. Corrosion 2004;60(9):824–36.

[11] Gabrielsen Ø, Larsen K, Reinholdtsen S-A. Fatigue testing of used mooring chain. In: International conference on ocean, offshore and arctic engineering, no. OMAE2017-61382. American Society of Mechanical Engineers Digital Collection; 2017.

[12] Gabrielsen Ø, Larsen K, Dalane O, Lie HB, Reinholdtsen S-A. Mean load impact on mooring chain fatigue capacity: Lessons learned from full scale fatigue testing of used chains. In: International conference on ocean, offshore and arctic engineering, no. OMAE2019-95083. American Society of Mechanical Engineers Digital Collection; 2019.
[13] Kondo Y. Prediction of fatigue crack initiation life based on pit growth. Corrosion 1989;45(1):7–11.
[14] Fernández J, Arredondo A, Storesund W, González JJ, et al. Influence of the mean load on the fatigue performance of mooring chains. In: Offshore technology conference, OTC-29621-MS. Offshore Technology Conference; 2019.
[15] Hobbacher AF. Recommendations for fatigue design of welded joints and components. Recommended guide IIW-2259-15, International Institute of Welding; 2016.
[16] DNV-GL. Fatigue design of offshore steel structures. Recommended guide DNVGL-RP-C203, DNV-GL; 2016.
[17] BSI. Guide to fatigue design and assessment of steel products. Recommended guide BS 7608:2014, The British Standards Institution; 2014.
[18] Edwards G, Pacheco L. A Bayesian method for establishing fatigue design curves. Struct Saf 1984;2(1):27–38. http://dx.doi.org/10.1016/0167-4730(84)90005-5, URL https://www.sciencedirect.com/science/article/pii/0167473084900055.
[19] Mathisen J, Hørte T, Moe V, Lean W. Calibration of a fatigue limit state – joint industry project DeepMoor design methods for deep water mooring systems. DNV report 98–3110, DNV; 1998.
[20] White MJ. Corrosion fatigue testing of 76mm grade R3 & R4 studless mooring chain, H5787/NDAI/MJW, rev 0. Technical report, Joint Industry Report. Noble Denton Associates, Inc.; 2002.
[21] DNV-GL. Offshore mooring chain. Offshore standard DNVGL-OS-E302, DNV-GL; 2018.
[22] Zarandi EP, Skallerud BrH. Experimental and numerical study of mooring chain residual stresses and implications for fatigue life. Int J Fatigue 2020;135:105530.
[23] Vasudevan A, Sadananda K. Classification of environmentally assisted fatigue crack growth behavior. Int J Fatigue 2009;31(11):1696–708. http://dx.doi.org/10.1016/j.ijfatigue.2009.03.019, URL http://www.sciencedirect.com/science/article/pii/S0142112309001236.
[24] Zhang Y, Zettlemoyer N, Tubby P. Fatigue crack growth rates of mooring chain steels. In: International conference on ocean, offshore and arctic engineering, no. OMAE2012-84223. American Society of Mechanical Engineers Digital Collection; 2012.
[25] Hudak Jr. SJ, Feiger JH, Patton JA. The effect of cyclic loading frequency on corrosion-fatigue crack growth in high-strength riser materials. In: International conference on ocean, offshore and arctic engineering, no. OMAE2010-20705; 2010.
[26] API. 6Th edition, specification for mooring chain. Standard API SPEC 2F, API; 1997.
[27] Zarandi EP, Skallerud BrH. Cyclic behavior and strain energy-based fatigue damage analysis of mooring chains high strength steel. Mar Struct 2020;70:102703.
[28] Ma K-t, Gabrielsen Ø, Li Z, Baker D, Yao A, Vargas P, Luo M, Izadparast A, Arredondo A, Zhu L, et al. Fatigue tests on corroded mooring chains retrieved from various fields in offshore west africa and the north sea. In: International conference on ocean, offshore and arctic engineering, no. OMAE2019-95618. American Society of Mechanical Engineers Digital Collection; 2019.
[29] Gelman A, Hill J. Data analysis using regression and multilevel/hierarchical models. Cambridge University Press; 2006.
[30] Laird NM, Ware JH. Random-effects models for longitudinal data. Biometrics 1982;963–74.
[31] Pearl J. Causality. Cambridge University Press; 2009.
[32] Melchers RE, Moan T, Gao Z. Corrosion of working chains continuously immersed in seawater. J Marine Sci Technol 2007;12(2):102–10.
[33] Zhang Y-H, Smedley P. Fatigue performance of high strength and large diameter mooring chain in seawater. In: International conference on ocean, offshore and arctic engineering, no. OMAE2019-95984. American Society of Mechanical Engineers Digital Collection; 2019.
[34] Fernández J, Storesund W, Navas J. Fatigue performance of grade R4 and R5 mooring chains in seawater. In: International conference on ocean, offshore and arctic engineering, no. OMAE2014-23491. American Society of Mechanical Engineers Digital Collection; 2014.
[35] Dowling NE. Mechanical behavior of materials: engineering methods for deformation, fracture, and fatigue. 4th ed.. Boston, Mass: Pearson Education; 2013.
[36] Mathworks: Linear mixed-effects models. 2021, https://www.mathworks.com/help/stats/linear-mixed-effects-models.html [Accessed 08 July 2021].
[37] JCSS. Probabilistic model code. Part 3: Resistance models. Joint Committee of Structural Safety; 2001.
[38] Sørensen JD. Reliability-based calibration of fatigue safety factors for offshore wind turbines. In: The twenty-first international offshore and polar engineering conference. International Society of Offshore and Polar Engineers; 2011.
[39] Madsen HO. Stochastic modeling of fatigue crack growth and inspection. In: Probabilistic methods for structural design. Springer; 1997, p. 59–83.
[40] Moan T, Song R. Implications of inspection updating on system fatigue reliability of offshore structures. J Offshore Mech Arct Eng 2000;122(3):173–80.
[41] Haagensen PJ, Köhler J. Fatigue testing of mooring chains - statistical analysis of data from test series with different number of chain links. Dept. of Structural Engineering, NTNU; 2015.